Sound velocities of Fe and Fe-Si alloy in the Earth's core

Zhu Mao[a,1], Jung-Fu Lin[a], Jin Liu[a], Ahmet Alatas[b], Lili Gao[b], Jiyong Zhao[b], and Ho-Kwang Mao[c]

[a]Department of Geological Sciences, Jackson School of Geosciences, University of Texas at Austin, Austin, TX 78712; [b]Advanced Photon Source, Argonne National Laboratory, Argonne, IL 60439; and [c]High Pressure Collaborative Access Team, Geophysical Laboratory, Carnegie Institution of Washington, Washington, DC 20015

Compressional wave velocity-density ($V_P - \rho$) relations of candidate Fe alloys at relevant pressure-temperature conditions of the Earth's core are critically needed to evaluate the composition, seismic signatures, and geodynamics of the planet's remotest region. Specifically, comparison between seismic $V_P - \rho$ profiles of the core and candidate Fe alloys provides first-order information on the amount and type of potential light elements—including H, C, O, Si, and/or S—needed to compensate the density deficit of the core. To address this issue, here we have surveyed and analyzed the literature results in conjunction with newly measured $V_P - \rho$ results of hexagonal closest-packed (hcp) Fe and hcp-$Fe_{0.85}Si_{0.15}$ alloy using in situ high-energy resolution inelastic X-ray scattering and X-ray diffraction. The nature of the Fe-Si alloy where Si is readily soluble in Fe represents an ideal solid-solution case to better understand the light-element alloying effects. Our results show that high temperature significantly decreases the V_P of hcp-Fe at high pressures, and the Fe-Si alloy exhibits similar high-pressure $V_P - \rho$ behavior to hcp-Fe via a constant density offset. These $V_P - \rho$ data at a given temperature can be better described by an empirical power-law function with a concave behavior at higher densities than with a linear approximation. Our new datasets, together with literature results, allow us to build new $V_P - \rho$ models of Fe alloys in order to determine the chemical composition of the core. Our models show that the $V_P - \rho$ profile of Fe with 8 wt % Si at 6,000 K matches well with the Preliminary Reference Earth Model of the inner core.

compressional-wave velocity | high pressure-temperature

Enigmatic properties of the Earth's inner core have recently been discovered including differential super-rotation (1), seismic anisotropies (2–4), and fine-scale seismic heterogeneities (5, 6). Deciphering these observations requires solid knowledge about the composition of the Earth's inner core and, therefore, the elasticity of candidate Fe alloys (7–16). Since F. Birch pointed out in the 1950s that Earth's core is too dense if composed of Fe or Fe-Ni alloy alone (13), a number of candidate major light elements, including oxygen (O), silicon (Si), sulfur (S), carbon (C), and hydrogen (H), have been suggested via cosmochemical, geochemical, and geophysical evidence (17). To ascertain the identity and exact amount of light elements needed in the Earth's inner core, one key piece of information lies in the comparison of the seismic $V_P - \rho$ profiles with reliable laboratory measurements of these properties for candidate Fe alloys. Potential Fe-light element alloy must have $V_P - \rho$ profiles that match seismic models such as the Preliminary Reference Earth Model and AK135 (7, 8). Thus, this requires precise experimental results describing the $V_P - \rho$ relationships of Fe alloys at pressure-temperature (P-T) conditions relevant to the Earth's core. To address this issue, here we present new experimental measurements on the $V_P - \rho$ relations of hcp-Fe and hcp-$Fe_{0.85}Si_{0.15}$ alloy at high P-T conditions using high-energy resolution inelastic X-ray scattering (HERIX) and X-ray diffraction (XRD) in an externally-heated diamond anvil cell (EHDAC). Si, unlike other candidate light elements with extremely limited solubility in Fe, readily alloys with Fe in the hcp structure at high P-T conditions (18),

though at 1 bar, 2 wt % C can dissolve in solid Fe but in the face-centered cubic structure (12). In this case, Si is ideally suited to understand the alloying effects on the $V_P - \rho$ relation of Fe (e.g., refs. 18 and 19). Together with our new experimental results, we have critically assessed existing literature results on the $V_P - \rho$ profiles of the Fe alloys. These results allow us to further model the $V_P - \rho$ relation of Fe alloys in order to evaluate the composition of the core at relevant P-T conditions.

Results and Discussion

Sound Velocities of Fe and Fe$_{0.85}$Si$_{0.15}$. We have conducted HERIX and XRD measurements to determine the $V_P - \rho$ relation of hcp-Fe up to 105 GPa and 700 K at Sector 3 of the Advanced Photon Source (APS), Argonne National Laboratory in an EHDAC (20, 21) (Fig. 1 *A* and *B*). The $V_P - \rho$ relation of hcp-$Fe_{0.85}Si_{0.15}$ (7.9 wt % Si), in which Si forms a solid solution with Fe in the hcp structure at high P-T (18), has also been determined up to 98 GPa at 300 K as a case study to understand the light-element alloying effects (Fig. 1*C*). The obtained phonon dispersion curves from HERIX measurements were fitted to a sine function within the framework of the Born–von Karman lattice-dynamics theory to derive the V_P of hcp-Fe and hcp-$Fe_{0.85}Si_{0.15}$ with uncertainties typically in the order of 1% or less (10, 20, 21) (Fig. 1, Figs. S1 and S2, and Tables S1 and S2). Measuring V_P and ρ simultaneously and precisely permits us to reliably establish the $V_P - \rho$ relation without using any external parameters, allowing more direct implications of the results to the core.
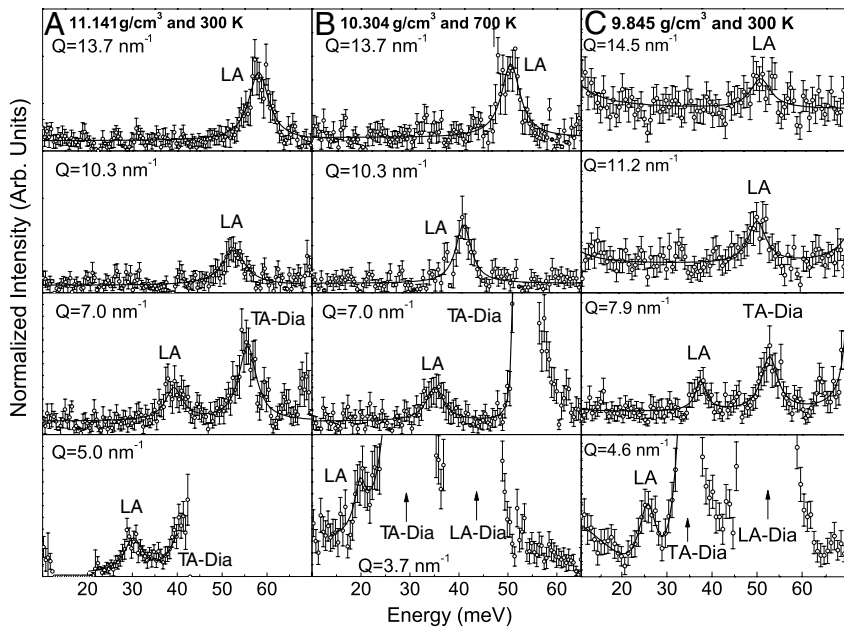
The measured V_P of hcp-Fe was strongly reduced at an elevated temperature of 700 K even at a constant density (Fig. 2). Due to the extremely small error bars in our $V_P - \rho$ data, we can resolve that the high-temperature effect was gradually suppressed by increasing density, likely as a result of the smaller thermal expansion coefficient at higher densities (thus less anharmonic effect) (22, 23). We observed a V_P decrease of 5.4($\pm$1.0)% from 300 to 700 K at a constant density of 9.256($\pm$0.004) g/cm^3, but the reduction over the same temperature span is only 2.9($\pm$1.0)% at the maximum density of 10.304($\pm$0.004) g/cm^3 (Fig. 2). Such reduction in V_P at high temperatures has been reported in a recent nuclear resonant inelastic X-ray scattering (NRIXS) study, but the scattering of the results has limited their implications to quantify the high P-T effect (22).

Besides the strong temperature effect on the V_P of hcp-Fe, we also noted that the V_P exhibits a downward trend toward higher densities (Fig. 2) and deviates from the linear function, so-called Birch's law (24). As noted by a number of previous studies and shown in our $V_P - \rho$ plot, the linear function may represent the $V_P - \rho$ behavior of planetary materials only within a limited pres-

EARTH, ATMOSPHERIC, AND PLANETARY SCIENCES

Fig. 1. Representative inelastic X-ray scattering spectra of hcp-Fe and hcp-Fe$_{0.85}$Si$_{0.15}$. (*A*) hcp-Fe at 105 GPa [corresponding to $\rho = 11.141(\pm0.008)$ g/cm^3] at 300 K. (*B*) hcp-Fe at 67 GPa [corresponding to $\rho = 10.304(\pm0.004)$ g/cm^3] and 700 K. (*C*) hcp-Fe$_{0.85}$Si$_{0.15}$ at 82 GPa [corresponding to $\rho = 9.845$ (±0.005) g/cm^3] and 300 K. Pressures were calculated using the equation of state of hcp-Fe (29, 30) and hcp-Fe$_{0.85}$Si$_{0.15}$ (35). Experimental data in open circles with error bars were fitted with a Lorentzian function (solid lines) for the longitudinal acoustic phonon peak (LA). Transverse acoustic phonon peaks (TA) from diamond anvils were observed when the momentum transfer (Q) was lower than approximately 8 nm^{-1}.

sure range, whereas a correction factor is needed to account for the higher pressure (density) effect on the V_P at a given temperature (25–28) (Fig. 2). We found that an empirical power-law function can be used to satisfactorily describe our $V_P - \rho$ data of hcp-Fe (26–28):

$$V_P = C(M)(\rho + a(T))^{\lambda},\qquad[1]$$

where $C(M)$ is an atomic mass constant at a given temperature, λ is a correction factor for the nonlinear behavior of the $V_P - \rho$ relationship (see *SI Methods*) (26–28), and $a(T)$ is a temperature-dependent correction factor that is given to account for the high-temperature effect on the V_P at higher densities. Assuming a linear $V_P - \rho$ relationship [by removing $a(T)$ and λ in the equation], on the other hand, would result in an overestimation of the V_P by 1.4% at our maximum experimental density of 11.141(±0.008) g/cm^3 (approximately 105 GPa using the equation of state parameters given in refs. 29 and 30) (Fig. 2). Comparison of our hcp-Fe and Fe-Si alloy results with previous studies on Fe at high pressures showed that hcp-Fe$_{0.85}$Si$_{0.15}$ systematically exhibits much higher V_P and much lower ρ than hcp-Fe (10, 31–34) (Fig. 2). The overall alloying effects of Si in Fe have resulted in reduced density and increased velocity at high pressures. Systematic $V_P - \rho$ comparisons between hcp-Fe$_{0.85}$Si$_{0.15}$ and hcp-Fe clearly show that the addition of Si mainly contributes to the density reduction in the $V_P - \rho$ relation of hcp-Fe at high pressures, as the $V_P - \rho$ line of hcp-Fe$_{0.85}$Si$_{0.15}$ matches well with that of hcp-Fe with a density decrease of approximately 1 g/cm^3 (Fig. 2). This density reduction behavior has been reported to occur in the body-centered cubic (bcc) Fe-Si alloy at ambient conditions (35). The finding on the solid-solution alloying effect on the $V_P - \rho$ profile permits one to extrapolate and to interpolate experimental data to higher pressures with more confidence.

Sound Velocities of Fe Alloys. In the past few decades, various techniques, including synchrotron XRD (29, 30), NRIXS (11, 22, 36, 37), HERIX (10, 31–33, 38, 39), and impulsive stimulated light scattering (ISLS) (40), combined with DACs, have been applied to measure the V_P of Fe-light element alloys at high pressures (Fig. 3*A*). Although large systematic uncertainties exist in comparison to each dataset (10, 11, 22, 23, 41–43), the V_P data of hcp-Fe generally seem to follow an empirical linear $V_P - \rho$ relation, so-called Birch's law, for the first-order approximation

without considering potential high-temperature anharmonic and higher pressure effects (10, 11) (Fig. 3*A*). Without higher *P-T* data, extrapolation and interpolation of the linear relationships in Fe alloys have been extensively used to estimate the amount and identity of light elements in the core. Nevertheless, high temperatures are reported to result in reduced sound velocities of hcp-Fe and Fe$_3$C in high *P-T* NRIXS measurements (22, 44) and in theoretical calculations (4). However, NRIXS is relatively sensitive to the shear-wave velocity, V_S, and much less sensitive
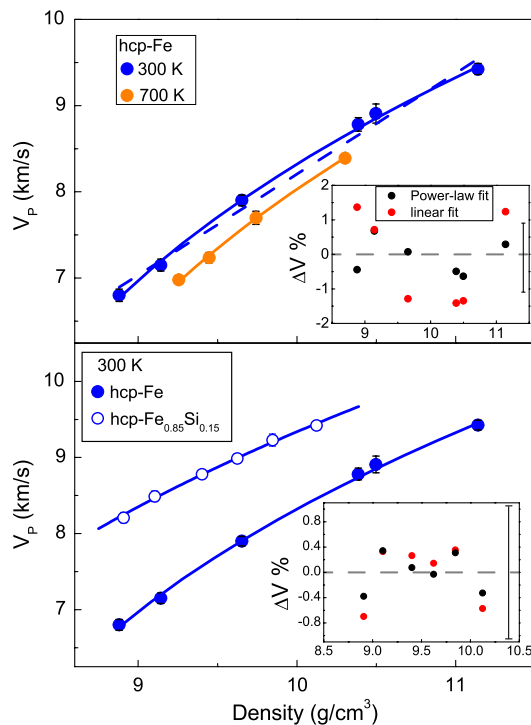
Fig. 2. $V_P - \rho$ of hcp-Fe and hcp-Fe$_{0.85}$Si$_{0.15}$ at high pressures and temperatures. (*A*) hcp-Fe. Dashed lines: linear fitting at 300 K; solid lines: the power-law fitting. (*B*) hcp-Fe (solid circles) and hcp-Fe$_{0.85}$Si$_{0.15}$ (open circles). Insert figure: deviations of the power-law fit (black circles) and the linear fit (red circles) from the experimental V_P of hcp-Fe (Fig. 2*A*) or hcp-Fe$_{0.85}$Si$_{0.15}$ (Fig. 2*B*) at high pressures and 300 K. Error bars for V_P in the order of 1% or less are smaller than the circles and are not shown (see Table S1 for details).
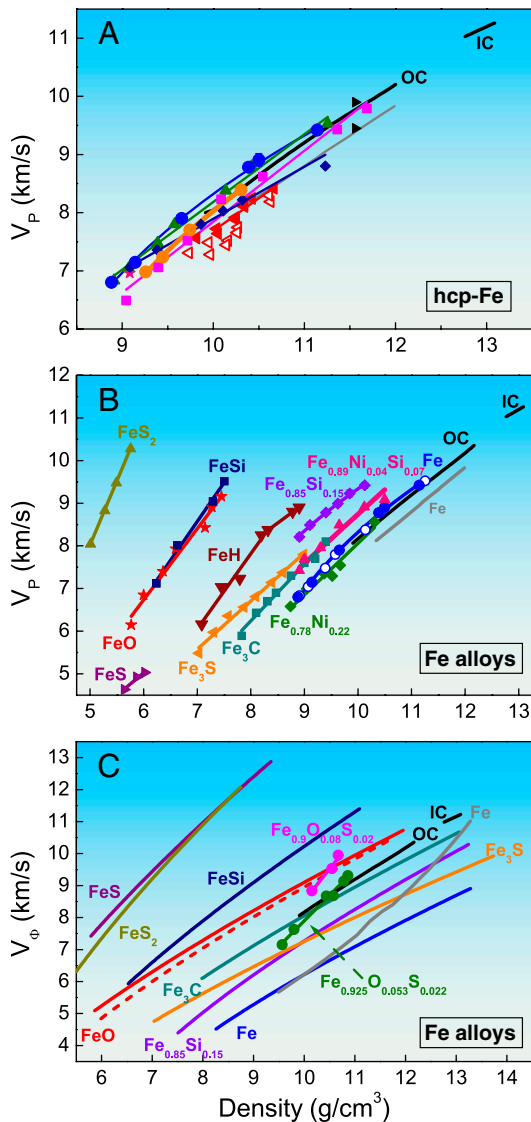
Fig. 3. Sound velocities of Fe and Fe alloys. (*A*) $V_P - \rho$ of hcp-Fe. Pink stars: ultrasonic measurements at ambient conditions (11); magenta squares: NRIXS measurements at high pressures and 300 K (11); olive triangles: ISLS measurements (40); royal diamonds: HERIX measurements (10); solid red left triangles: NRIXS measurements at 300 K (22); open red left triangles: NRIXS measurements at high *P-T* (22); black right triangles: HERIX measurements from highly textured hcp-Fe (38); black lines: Earth's outer core (OC) and inner core (IC) from seismic model AK135 (8), respectively; grey lines: shock wave measurements (23, 40). Respective color lines are linear or power-law fits to the data. (*B*) V_P of Fe alloys. Blue solid circles: hcp-Fe from this study; open circles: hcp-Fe (40); violet diamonds: $Fe_{0.85}Si_{0.15}$ from this study; olive diamonds: $Fe_{0.78}Ni_{0.22}$ (31); pink triangles: $Fe_{0.89}Ni_{0.04}Si_{0.07}$ (32); dark cyan squares: Fe_3C (37); orange left triangles: Fe_3S (36); purple right triangles: FeS (33); red stars: FeO (33); navy squares: FeSi (33); dark yellow triangles: FeS_2 (33); wine down triangles: FeH (39). (*C*) Bulk sound velocity (V_Φ) of Fe alloys. Solid lines, except the black and grey lines, are the V_Φ of Fe alloys calculated from static compression results at 300 K. Blue line: hcp-Fe (29, 30); orange line: Fe_3S (50, 51); violet line: $Fe_{0.85}Si_{0.15}$ (35, 51, 52); dark cyan line: Fe_3C (53, 54); red solid and dashed lines: FeO in B1 and B8 phase, respectively (55); navy blue line: FeSi (55, 56); purple line: FeS in the IV phase (53, 57); magenta and olive circles: V_Φ of $Fe_{0.9}O_{0.08}S_{0.02}$ and $Fe_{0.925}O_{0.053}S_{0.022}$ from shock-compression study, respectively (15).

to V_P, a better-constrained seismic parameter, thus limiting its direct implications to the inner core geochemistry (11, 22).

Comparison between $V_P - \rho$ of hcp-Fe and Earth's core indicates significant $V_P - \rho$ differences that call for the addition of approximately 8–10 wt % light elements in the outer core and 4 wt % in the inner core (e.g., 12–15, 23) (Fig. 3*B*). The amount of Ni in the core is approximately 5–15 wt % (14, 45) that likely would not significantly affect the $V_P - \rho$ relation of Fe (31) (Fig. 3*B*). On the other hand, adding a certain amount of light elements can significantly decrease the density and increase the sound velocities [V_P and bulk sound velocity (V_Φ)] of Fe, providing a better match for the $V_P - \rho$ profile of the Earth's core (31–33, 36, 38–40) (Fig. 3 *B* and *C*). Fig. 3*B* summarizes the $V_P - \rho$ profiles of Fe-light element alloys (H, C, O, Si, and S) at high pressures from recent laboratory measurements (31–33, 36, 38–40) together with our new experimental results. All of these light elements seem to produce some degree of alloying effects on the $V_P - \rho$ profiles that could be interpolated with the Fe profile to match that of the Earth's core for the first-order approximation, though end-member FeS_2, FeSi, FeH, and FeO compounds exhibit much higher V_P slopes than Fe and Earth's core. Indeed, with the exception of Si, these light elements have extremely limited solubility in Fe at ambient conditions and, thus, exist with Fe as end-member or intermediate compounds in various structural forms (12). Structural transitions have been shown to affect the $V_P - \rho$ trend significantly at high pressures (25), suggesting that the $V_P - \rho$ profiles of end-member compounds should be exercised with caution especially under the extreme *P-T* conditions of the core. For instance, FeO is stable in the cesium chloride (CsCl)-type (B2) phase at the expected *P-T* conditions of the Earth's inner core (46), yet, the $V_P - \rho$ relationship of FeO has only been studied for the rhombohedral-B1 phase (33) (Fig. 3 *B* and *C*). Estimation on the O content based on the $V_P - \rho$ profile of the rhombohedral-B1 FeO may thus introduce large uncertainties. Similarly, the $V_P - \rho$ profile of FeS has only been determined for the hexagonal NiAs-type phase (IV) (33), although FeS transforms to a CsCl-type B2 phase (VII) at above 180 GPa and high temperatures (47, 48). A given light element could be incorporated into different structural forms of Fe with very different $V_P - \rho$ relationships, making the estimation on the amount of light elements in the Earth's core much more complicated. For instance, Badro et al. (33) reported the V_P of FeS and FeS_2 as a function of ρ at high pressures. By linearly extrapolating the obtained $V_P - \rho$ relations of Fe and Fe alloys to the relevant *P-T* conditions of the core. However, the S content is estimated to be 3.9 wt % in the core, if S exists as FeS_2. This estimated amount can be as high as 9.7 wt % for the FeS phase. The same argument also applies to Fe-C compounds such as Fe_3C and Fe_7C_3 (37, 49), in which the $V_P - \rho$ relation of Fe_3C has been investigated experimentally (37, 44).

In addition to the $V_P - \rho$ profiles, static XRD and shock-compression studies have provided constraints on the $V_\Phi - \rho$ relations of Fe alloys (18, 29, 30, 50–57) (Fig. 3*C*). It should be noted that pressure-volume relations, instead of $V_\Phi - \rho$, were measured in XRD experiments, whereas temperature measurements along Hugoniot shock compressions were largely uncertain, leading to potential uncertainties in the $V_\Phi - \rho$ data. Recently, Huang et al. (15) have measured the $V_\Phi - \rho$ profiles of two Fe-S-O alloys using shock-compression technique. The $V_\Phi - \rho$ profile of the sulfur-rich and oxygen-poor Fe alloy ($Fe_{0.925}O_{0.053}S_{0.022}$) matches that of the outer core, whereas the $V_\Phi - \rho$ profile of an oxygen-rich Fe-S-O alloy ($Fe_{0.9}O_{0.08}S_{0.02}$) deviates from that of the outer core, indicating that oxygen can be ruled out as a major light element in the Earth's outer core. Based on the aforementioned discussions on literature results, it is critical to have reliable velocity-density profiles of Fe solid-solution alloys at simultaneous high *P-T* conditions in the hcp crystal structure in order to evaluate more accurately the composition of the Earth's core.

Density Deficits of Fe Alloys. Using the new $V_P - \rho$ profiles of hcp-Fe and Fe-Si alloy, together with the literature results, we have evaluated the density deficits at high pressures (Fig. 4).
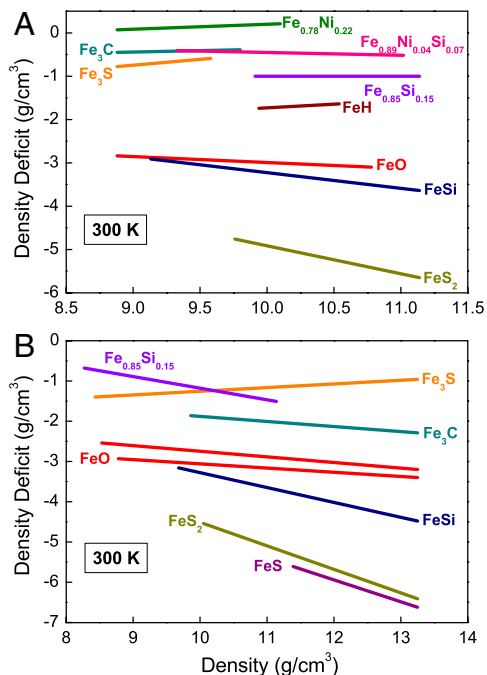
Fig. 4. Density deficits of Fe alloys with respect to hcp-Fe. (*A*) density deficit derived from the $V_P - \rho$ profile. Violet line: $Fe_{0.85}Si_{0.15}$ from this study; olive line: $Fe_{0.78}Ni_{0.22}$(31); pink line: $Fe_{0.89}Ni_{0.04}Si_{0.07}$(32); dark cyan line: Fe_3C (37); orange line: Fe_3S (36); red line: FeO (33); wine line: FeH (39); navy blue line: FeSi (33); dark yellow line: FeS_2 (33). The overall uncertainty of these density deficits is approximately 0.05 g/cm^3. (*B*) density deficit derived from the $V_\Phi - \rho$ profile. Orange line: Fe_3S (50, 51); violet line: $Fe_{0.85}Si_{0.15}$ (35, 51, 52); dark cyan line: Fe_3C (53, 54); red solid and dashed lines: FeO in B1 and B8 phase, respectively (55); navy blue line: FeSi (48, 56); purple line: FeS in phase IV structure (48, 57). The overall uncertainty of these density deficits is approximately ±0.01 g/cm^3.

The density deficit of each Fe alloy system is obtained by using our $V_P - \rho$ profile of hcp-Fe as the reference (Fig. 4*A*). At a given V_P, the density deficit is defined by the density difference between the Fe-light element alloy and the hcp-Fe. Comparison of the deficits shows that adding Ni into Fe marginally increases the density (32), whereas all candidate light elements decrease the density of hcp-Fe (31–33, 36, 37, 39). The density deficit of hcp-$Fe_{0.85}Si_{0.15}$ is fairly independent of the density increase, though Fe_3C, Fe_3S, and FeH systems seem to show a marginally positive slope (33, 37, 39), whereas FeO displays a negative slope (33). We have also calculated the density deficits of Fe alloys using the $V_\Phi - \rho$ profiles from the XRD measurements following the same method to derive the density deficits from the $V_P - \rho$ profiles (29, 30, 35, 50–58) (Fig. 4*B*). With the exceptions of the Fe_3C and $Fe_{0.85}Si_{0.15}$, the density deficit of FeO, FeSi, and Fe_3S, determined from the $V_\Phi - \rho$ profile, follow a similar trend with that determined from the $V_P - \rho$ profile.

New $V_P - \rho$ Profiles of Fe and Fe-Si Alloy in the Earth's Inner Core: Implication for the Core Composition. As shown from our high P-T measurements and previous NRIXS study (22, 44), the effect of temperature at a given pressure on the sound velocity of Fe cannot be ignored. Here we have applied our results to establish a new $V_P - \rho$ model of hcp-Fe and hcp-$Fe_{0.85}Si_{0.15}$ at relevant P-T conditions of the inner core. The new $V_P - \rho$ model aims to provide preliminary constraints on the composition of the inner core and to examine how the variation in temperature can affect our understanding of the core composition by using a solid-solution Fe-Si alloy in the hcp structure as an example. Our experimental results are extrapolated to relevant inner core conditions using the power-law function and previous shock wave results
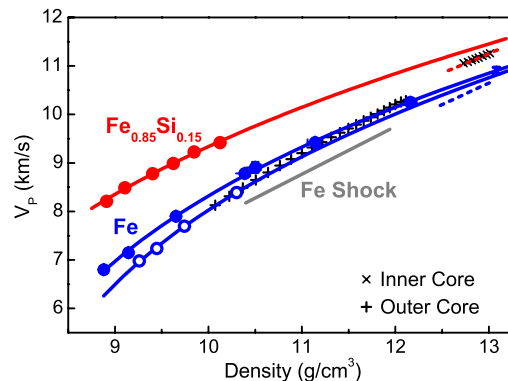
Fig. 5. Modeled $V_P - \rho$ relation of hcp-Fe in Earth's core. Blue solid lines: modeled V_P at 300 K (solid circles) and 700 K (open circles) of hcp-Fe from the power-law function, respectively; red solid line: modeled V_P at 300 K of hcp-$Fe_{0.85}Si_{0.15}$ from the power-law function; blue and red dashed lines: $V_P - \rho$ 6,000 K derived from the measured V_P in this study and shock-compression measurements of hcp-Fe and hcp-$Fe_{0.85}Si_{0.15}$, respectively (23, 41); grey line: shock-compression measurements of hcp-Fe (23, 41); black pluses (+) and crosses (×): seismic observations for the outer and inner core (8), respectively.

(Fig. 5 and see *SI Text* for details) (23, 41). Our model shows that power-law extrapolated V_P of hcp-Fe at 300 K is 5–6% and 3.5% lower than that of the linear extrapolation and seismic references, respectively, whereas V_P of hcp-$Fe_{0.85}Si_{0.15}$ at 300 K are 6.2–7% lower than that of the linear extrapolation but 2% greater than that of the seismic references (7, 8, 10, 33) (Fig. 5). Considering the high-temperature effect on the V_P reduction of hcp-Fe, our $V_P - \rho$ model of hcp-Fe at 6,000 K is 6% lower than the seismic models (7, 8) (Fig. 5), whereas the extrapolated $V_P - \rho$ line of hcp-$Fe_{0.85}Si_{0.15}$ at 6,000 K is consistent with the seismic models of the inner core. Furthermore, the $V_P - \rho$ line of hcp-$Fe_{0.85}Si_{0.15}$ exhibits a similar slope to the seismic models (Fig. 5). That is, the $V_P - \rho$ profile of hcp-Fe with approximately 8 wt. % Si ($Fe_{0.85}Si_{0.15}$) at 6,000 K can satisfactorily explain the seismic $V_P - \rho$ of the inner core.

Based on our model, the percentage of light elements such as Si in the inner core can be assessed by comparing the seismically known relationship between V_P and ρ with laboratory measurements for candidate Fe alloys. The linear $V_P - \rho$ relationship and ideal solid-solution behavior of candidate Fe alloys has been commonly assumed in order to extrapolate experimental results to the inner core pressures (33). This linear model, however, does not take the non-linear $V_P - \rho$ behavior and high-temperature anharmonic effects into account, and would overestimate the amount of a candidate light element needed in the inner core. For example, extrapolation of our $V_P - \rho$ data using a linear model would result in much higher V_P than the power-law model, requiring more than 10 wt. % Si in the inner core. This amount of Si is much higher than the estimate in the power-law model and is inconsistent with recent cosmochemical and geochemical constraints (19, 59–65). Direct measurements of the $V_P - \rho$ relationship of Fe-light element alloys at relevant P-T conditions of the core now appear to be on the horizon, which in turn may eventually answer the longstanding question on the composition of the Earth's core.

Methods

Polycrystalline Fe and $Fe_{0.85}Si_{0.15}$ alloys were used as the starting samples. The Fe-Si alloy was obtained from Goodfellow Corporation (lot FE166010/6); details of the sample have been given elsewhere (18, 35). Electron microprobe analyses showed that the Fe sample did not contain any detectable impurities and the Fe-Si sample contained 7.9 (±0.3) wt % Si homogeneously, whereas XRD spectra showed that both samples were in the body-centered cubic (bcc) structure.

The Fe sample was sandwiched between two NaCl layers or loaded with Ne which served as a pressure medium and an insulating layer from the Re

gasket in EHDAC, whereas the $Fe_{0.85}Si_{0.15}$ alloy was loaded with Ne. For EHDAC with Fe sample, the temperature (700 K) was measured by a K-type thermocouple placed on the diamond's surface close to the sample. For HER-IX measurements at sector 3 of the APS, an incident X-ray beam with an energy of 21.657 keV and an energy bandwidth of 2.3 meV was focused to a beamsize of 15 μm vertically and 22 μm horizontally. Phonon-dispersion spectra with an energy resolution of approximately 2.3 meV were simultaneously collected by detectors with four spherical silicon crystal analyzers with a collection time between 12 and 24 h (Fig. 1). The X-ray beam was also used for in situ XRD measurements to determine the sample densities. Potential differential stress of the Fe sample was further reduced by annealing the sample at 700 K for a few hours before the data collection.

$Fe_{0.85}Si_{0.15}$ sample measuring approximately 22 μm thick and 50 μm in diameter was loaded into a symmetric DAC with 300 μm culets of diamonds for measurements at 39 GPa, 47 GPa, and 60 GPa, whereas another sample measuring approximately 22 μm thick and 50 μm in diameter was loaded into another symmetric DAC with 150–300 μm beveled diamond culets for measurements at 71, 82, and 98 GPa (Fig. S1). The choice of the sample thickness and diameter was intended to provide optimal HERIX signals while sampling a smaller pressure gradient across the sample and a much lesser signal from Ne medium. Orientations of the diamonds were predetermined using Brillouin light scattering and Raman spectroscopy, and were prealigned such that the fastest transverse acoustic waves (TA) of the diamonds were oriented along the momentum transfer of the HERIX measurements. This permits better separation of the sample longitudinal acoustic wave (LA) from the TA dispersion curve of the diamond especially at higher pressures where phonon dispersion curves of the sample are expected to occur at higher energy transfers (Fig. 1 and Fig. S1).

1. Creager KC (1997) Inner core rotation rate from small-scale heterogeneity and time-varying travel times. *Science* 278:1284–1288.
2. Stixrude L, Cohen RE (1995) High-pressure elasticity of iron and anisotropy of Earth's inner core. *Science* 267:1972–1975.
3. Steinle-Neumann G, et al. (2001) Elasticity of iron at the temperature of the Earth's inner core. *Nature* 413:57–60.
4. Sha X, Cohen RE (2010) Elastic isotropy of ε-Fe under Earth's core conditions. *Geophys Res Lett* 37:L10302.
5. Niu F, Wen L (2001) Hemispherical variations in seismic velocity at the top of the Earth's inner core. *Nature* 410:1081–1084.
6. Alboussière T, Deguen R, Melzani M (2010) Melting-induced stratification above the Earth's inner core due to convective translation. *Nature* 466:744–747.
7. Dziewonski AM, Anderson DL (1981) Preliminary reference earth model. *Phys Earth Planet Inter* 25:297–356.
8. Kennett BLN, Engdahl ER, Buland R (1995) Constraints on seismic velocities in the Earth from travel times. *Geophys J Int* 122:108–124.
9. Song X, Helmberger DV (1995) A P wave velocity model of Earth's core. *J Geophys Res* 100:9817–9830.
10. Fiquet G, et al. (2001) Sound velocities in iron to 110 gigapascals. *Science* 291:468–471.
11. Mao HK, et al. (2001) Phonon density of states of iron up to 153 gigapascals. *Science* 292:914–916.
12. Li J, Fei Y (2003) Experimental constraints on core composition. *Treatise on Geochemistry*, eds RW Carlson, HD Holland, and KK Turekian (Elsevier-Pergamon, Oxford), 2, pp 521–546.
13. Birch F (1952) Elasticity and constitution of the Earth's interior. *J Geophys Res* 57:227–286.
14. McDonough WF (2003) Compositional model for the Earth's core. *Treatise on Geochemistry*, eds HD Holland and KK Turekian (Elsevier-Pergamon, Oxford), 2, pp 547–568.
15. Huang H, et al. (2011) Evidence for an oxygen-depleted liquid outer core of the Earth. *Nature* 479:513–516.
16. Duffy TS (2011) Probing the core's light elements. *Nature* 479:480–481.
17. Li J, Fei Y (2007) Experimental constraints on core composition. *Treatise on Geochemistry, Update 1*, eds HD Holland and KK Turekian (Elsevier-Pergamon, Oxford), Vol 2, pp 1–31.
18. Lin JF, et al. (2009) Phase relations of Fe-Si alloy in Earth's core. *Geophys Res Lett* 36:L06306.
19. Lin JF, et al. (2003) Sound velocities of iron-nickel and iron-silicon alloys at high pressures. *Geophys Res Lett* 30:2112.
20. Alatas A, et al. (2011) Improved focusing capacity for inelastic X-ray spectrometer at 3-ID of the APS: A combination of toroidal and Kirkpatrick-Baez (KB) mirror. *Nucl Instrum Methods Phys Res A* 649:166–168.
21. Toellner TS, et al. (2011) Six-reflection meV-monochromator for synchrotron radiation. *J Synchrotron Radiat* 18:605–611.
22. Lin JF, et al. (2005) Sound velocities of hot dense iron: Birch's law revisited. *Science* 308:1892–1894.
23. Brown JM, McQueen RG (1986) Phase transitions, Grüneisen parameter, and elasticity for shocked iron between 77 GPa and 400 GPa. *J Geophys Res* 91:7485–7494.
24. Birch F (1961) The velocity of compressional waves in rocks to 10 kilobars, part 2. *J Geophys Res* 66:2199–2224.
25. Campbell AJ, Heinz DL (1992) A high-pressure test of Birch's law. *Science* 257:66–67.
26. Chung DH (1972) Birch's law: Why is it so good. *Science* 177:261–263.
27. Anderson OL (1973) Comments on the power law representation of Birch's law. *J Geophys Res* 78:4901–4914.
28. Liebermann RC, Ringwood AE (1973) Birch's law and polymorphic phase transformations. *J Geophys Res* 78:6926–6932.
29. Mao HK, et al. (1990) Static compression of iron to 300 GPa and $Fe_{08}Ni_{0.2}$ alloy to 260 GPa: Implications for composition of the core. *J Geophys Res* 95:21,737–21,742.
30. Dewaele A, et al. (2006) Quasihydrostatic equation of state of iron above 2 Mbar. *Phys Rev Lett* 97:215504.
31. Kantor AP, et al. (2007) Sound wave velocities of fcc Fe-Ni alloy at high pressure and temperature by mean of inelastic X-ray scattering. *Phys Earth Planet Inter* 164:83–89.
32. Antonangeli D, et al. (2010) Composition of the Earth's inner core from high-pressure sound velocity measurements in Fe-Ni-Si alloys. *Earth Planet Sci Lett* 295:292–296.
33. Badro J, et al. (2007) Effect of light elements on the sound velocity of solid iron: Implications for the composition of Earth's core. *Earth Planet Sci Lett* 254:233–238.
34. Tsuchiya T, Fujibuchi M (2009) Effects of Si on the elastic property of Fe at Earth's inner core pressures: First principle study. *Phys Earth Planet Inter* 174:212–219.
35. Lin JF, Campbell AJ, Heinz DL (2003) Static compression of iron-silicon alloys: Implications for silicon in the Earth's core. *J Geophys Res* 108:2045.
36. Lin JF, et al. (2004) Magnetic transition and sound velocities of Fe_3S at high pressure: Implications for Earth and planetary cores. *Earth Planet Sci Lett* 226:33–40.
37. Gao L, et al. (2008) Pressure-induced magnetic transition and sound velocities of Fe_3C: Implications for carbon in the Earth's core. *Geophys Res Lett* 35:L17306.
38. Antonangeli D, et al. (2004) Elastic anisotropy in textured hcp-iron to 112 GPa from sound wave propagation measurements. *Earth Planet Sci Lett* 225:243–251.
39. Shibazaki Y, et al. (2012) Sound velocity measurements in dhcp-FeH up to 70 GPa with inelastic X-ray scattering: Implications for the composition of the Earth's core. *Earth Planet Sci Lett* 313–314:79–85.
40. Crowhurst JC, Goncharov AF, Zaug JM (2004) Impulsive stimulated light scattering from opaque materials at high pressure. *J Phys Condens Matter* 16:S1137–1142.
41. Nguyen JH, Holmes NC (2004) Melting of iron at the physical conditions of the Earth's core. *Nature* 427:339–342.
42. Stixrude L, Cohen RE (1995) High-pressure elasticity of iron and anisotropy of Earth's inner core. *Nature* 267:1972–1975.
43. Mao HK, et al. (1999) Elasticity and rheology of iron above 220 GPa and the nature of the Earth's inner core. *Nature* 399:741–743.
44. Gao L, et al. (2011) Effect of temperature on sound velocities of compressed Fe_3C, a candidate component of the Earth's inner core. *Earth Planet Sci Lett* 309:213–220.
45. Anderson D (1989) *Theory of Earth* (Blackwell Scientific Publications, Oxford), pp 63–78.
46. Ozawa H, et al. (2011) Phase transition of FeO and stratification in Earth's outer core. *Science* 334:792–794.
47. Ono S, et al. (2008) High-pressure phase transformation of FeS: Novel phases at conditions of planetary cores. *Earth Planet Sci Lett* 272:481–487.
48. Sata N, et al. (2008) New high-pressure B2 phase of FeS above 180 GPa. *Am Mineral* 93:492–494.
49. Mookherjee M, et al. (2011) High-pressure behavior of iron carbide (Fe_7C_3) at inner core conditions. *J Geophys Res* 116:B04201.
50. Seagle CT, Campbell AJ, Heinz DL, Shen G, Prakapenka VB (2006) Thermal equation of state of Fe_3S and implications for sulfur in Earth's core. *J Geophys Res* 111:B06209.
51. Chen B, et al. (2007) Thermal expansion of iron-rich alloys and implications for the Earth's core. *Proc Natl Acad Sci USA* 104:9162–9167.
52. Zhang J, Guyot F (1999) Thermal equation of state of iron and $Fe_{0.91}Si_{0.09}$. *Phys Chem Miner* 26:206–211.
53. Sata N, et al. (2010) Compression of FeSi, Fe_3C, $Fe_{0.95}O$, and FeS under the core pressures and implication for light element in the Earth's core. *J Geophys Res* 115:B09204.
54. Wood IG, et al. (2004) Thermal expansion and crystal structure of cementite, Fe_3C, between 4 and 600 K determined by time-of-flight neutron powder diffraction. *J Appl Crystallogr* 37:82–90.
55. Fischer RA, et al. (2011) Equation of state and phase diagram of FeO. *Earth Planet Sci Lett* 304:496–502.
56. Vočadlo L, et al. (2002) Thermal expansion and crystal structure of FeSi between 4 and 1173 K determined by time-of-flight neutron powder diffraction. *Phys Chem Miner* 29:132–139.
57. Tenailleau C, et al. (2005) Thermal expansion of troilite and pyrrhotite determined by in situ cooling (873 to 373 K) neutron powder diffraction measurements. *Mineral Mag* 69:205–216.

EARTH, ATMOSPHERIC, AND PLANETARY SCIENCES

Mao et al.

58. Vočadlo L (2007) Ab initio calculations of the elasticity of iron and iron alloys at inner core conditions: Evidence for a partially molten inner core. *Earth Planet Sci Lett* 254:227–232.
59. McDonough WF, Sun SS (1995) The composition of the Earth. *Chem Geol* 120:223–253.
60. Georg RB, et al. (2007) Silicon in the Earth's core. *Nature* 447:1102–1106.
61. Shahar A, et al. (2009) Experimentally determined Si isotope fractionation between silicate and Fe metal and implications for Earth's core formation. *Earth Planet Sci Lett* 288:228–234.
62. Javoy M, et al. (2010) The chemical composition of the Earth: Enstatite chondrite models. *Phys Earth Planet Inter* 293:259–268.
63. Armytage RMG, et al. (2011) Silicon isotopes in meteorites and planetary core formation. *Geochim Cosmochim Acta* 75:3662–3676.
64. Rubie DC, et al. (2011) Heterogeneous accretion, composition and core-mantle differentiation of the Earth. *Earth Planet Sci Lett* 301:31–42.
65. Tuff J, Wood BJ, Wade J (2011) The effect of Si on metal-silicate partitioning of siderophile elements and implications for the conditions of core formation. *Geochim Comoschim Acta* 75:673–690.

Supporting information

Mao et al. 10.1073/pnas.1207086109

SI Text

SI Methods. *Fitting the $V_P - \rho$ data.* Previous studies have shown that the power-law function can be derived from the fundamental Debye theory that relates the sound velocities to vibration frequencies or interatomic pair potentials (1–5) and can be used to describe sound velocity behaviors of rocks and minerals (1–5). It has been argued in these previous studies that the linear Birch's law is a representation of the power-law function over a limited range of density (1–5), providing a convenient means to evaluate the $V_P - \rho$ of rocks and minerals in the Earth's deep interior when experimental results are difficult to obtain. Here, we have developed a modified power-law function to account for the curved behavior of the $V_P - \rho$ relation of hcp-Fe at extended pressure-temperature (*P-T*) conditions:

$$V_P = C(M)(\rho + a(T))^{\lambda},\qquad \textbf{[S1]}$$

where $C(M)$ is the averaged atomic weight constant at a given temperature, and λ is a correction factor for the nonlinear behavior of the $V_P - \rho$. $a(T)$ is a temperature-dependent correction factor that is given to account for the high-temperature effect on the V_P at higher densities. Fitting the measured $V_P - \rho$ data using Eq. S1. (1) yields $C(M) = 6.3(\pm 0.6)$, $a(T) = -7.61$ (± 0.34), and $\lambda = 0.327(\pm 0.056)$ for our data at 300 K and $C(M) = 6.3$ (fixed), $a(T) = -7.88(\pm 0.06)$, and $\lambda = 0.332$ (± 0.018) at 700 K. For $Fe_{0.85}Si_{0.15}$, we obtained $C(M) = 6.2$ (± 0.4), $a(T) = -6.54(\pm 0.10)$, and $\lambda = 0.327$ (fixed).

***Power-law $V_P - \rho$ relation.*** We have applied our results to estimate the $V_P - \rho$ relation of the hcp-Fe and $Fe_{0.85}Si_{0.15}$ alloy at relevant *P-T* conditions of the inner core using the power-law function in Eq. S1 and shock-compression results (6, 7) in which values of $a(T)$ and λ are essential to construct the $V_P - \rho$ relation at a given temperature. For hcp-Fe, shock-compression studies provide additional constraints on the $a(T)$ and λ at high *P-T*. With known $V_P - \rho$ at a given *P-T* condition, deriving $a(T)$ and λ simultaneously following Eq. S1 would introduce significant uncertainties. As shown in our experimental results, high temperature strongly reduces V_P at a given density. With a fixed ρ value, V_P at the temperature T_i must be smaller (larger) than V_P at temperature T_{i-1} (T_{i+1}) where T_{i-1} (T_{i+1}) is lower (higher) than T_i. Using this as an additional constraint, we derived an upper and lower bound of $a(T_i)$, represented as $a(T_i)_{max}$ and $a(T_i)_{min}$, respectively. The difference in $a(T_i)_{max}$ and $a(T_i)_{min}$ is found to be less than 3%. The average value, $a(T_i)_{ave} = (a(T_i)_{max} + a(T_i)_{min})/2$ represents $a(T_i)$ at temperature T_i. On the other hand, λ is then retrieved from the power law representation in (1) with the known $a(T_i)$, V_P and ρ at a given *P-T* condition. Once $a(T_i)$ and λ are determined, the V_P value can be calculated at any given ρ.

A survey of the literature values on the melting curve of Fe at the outer-inner core boundary gives an averaged melting temperature of approximately 6,000 K that is used for the modeled temperature of the inner core. The ρ of the hcp-Fe can be calculated from literature equation of state parameters for the inner core *P-T* conditions (8). At a given density in the inner core conditions, ρ_c, the related V_P was found to decrease exponentially with temperature. Following this exponential function, we then computed the V_P of hcp-Fe at 6,000 K and the density of the inner core. For the $Fe_{0.85}Si_{0.15}$ alloy, we simply assumed that the effect of temperature on the V_P is the same as that on the hcp-Fe.

Nonhydrostaticity and texturing in the hcp-Fe sample. Previous high-energy resolution inelastic X-ray scattering (HERIX) experiments on hcp-Fe have been performed under nonhydrostatic conditions (9, 10) that have resulted in developments of strong textures in the sample. Radial X-ray diffraction studies of the hcp-Fe have showed that textures strongly developed up to ~50 GPa, but the maximum pole intensity of hcp-Fe only slightly increases with further pressure increase (11). It should be noted that under quasihydrostatic conditions, such as in the case of our experiments in NaCl or Ne medium, a certain amount of the basal lattice planes of the hcp-Fe crystals can also reorient perpendicularly to the maximum compression axis of the diamond anvil cell (the axial direction), resulting in some degrees of texturing in the sample. Nevertheless, analyses of the X-ray diffraction patterns of our hcp-Fe samples showed that these samples were not highly textured indicating that our measured V_P can be used to represent the sound velocity of the randomly oriented polycrystalline sample.

We have further compared our measured V_P with those from refs. 9 and 10 in Fig. S2. Considering the experimental setup in this study, the direction of the momentum transfer was perpendicular to the diamond anvil cell axis (the maximum compression axis). If the hcp-Fe is highly textured, the measured V_P would represent the velocity along the basal plane. As a result, our V_P along this direction should be more consistent with the V_P value of the highly textured samples along the same direction reported in Antonangeli et al. (10) at similar pressures. Indeed, linearly approximation and extrapolation of the V_P from Fiquet et al. (9) showed that the hcp-Fe sample used in Fiquet et al. (9) was highly textured. The obtained V_P in Fiquet et al. (9) thus cannot be used to represent the aggregate velocity of hcp-Fe. As shown in Fig. S2, the extrapolated V_P line from the linear and power-law functions is bracketed between the fast and slow velocities in Antonangeli et al. (10). Considering the texture analyses, quasihydrostatic environments and annealing of the sample, we thus conclude that the texturing of hcp-Fe has minimal effects on the reported V_P values in this study.

1. Anderson OL (1967) A seismic equation of state. *Geophys J Roy Astr S* 13:9–30.
2. Anderson OL (1973) Comments on the power law representation of Birch's law. *J Geophys Res* 78:4901–4914.
3. Shankland TJ (1972) Velocity-density systematics: Derivation from Debye theory and the effect of ionic size. *J Geophys Res* 77:3750–3758.
4. Chung DH (1972) Birch's law: Why is it so good. *Science* 177:261–263.
5. Liebermann RC, Ringwood AE (1973) Birch's law and polymorphic phase transformations. *J Geophys Res* 78:6926–6932.
6. Brown JM, McQueen RG (1986) Phase transitions, Grüneisen parameter, and elasticity for shocked iron between 77 GPa and 400 GPa. *J Geophys Res* 91:7485–7494.
7. Nguyen JH, Holmes NC (2009) Melting of iron at the physical conditions of the Earth's core. *Nature* 427:339–342.
8. Uchida T, Wang Y, Rivers ML, Sutton SR (2001) Stability field and thermal equation of state of ε-iron determined by synchrotron X-ray diffraction in a multianvil apparatus. *J Geophys Res* 106:21799–21810.
9. Fiquet G et al. (2001) Sound velocities in iron to 110 gigapascals. *Science* 291:468–471.
10. Antonangeli D et al. (2004) Elastic anisotropy in textured hcp-iron to 112 GPa from sound wave propagation measurements. *Earth Planet Sci Lett* 225:243–251.
11. Wenk HR et al. (2000) The plastic deformation of iron at pressures of the Earth's inner core. *Nature* 405:1044–1047.
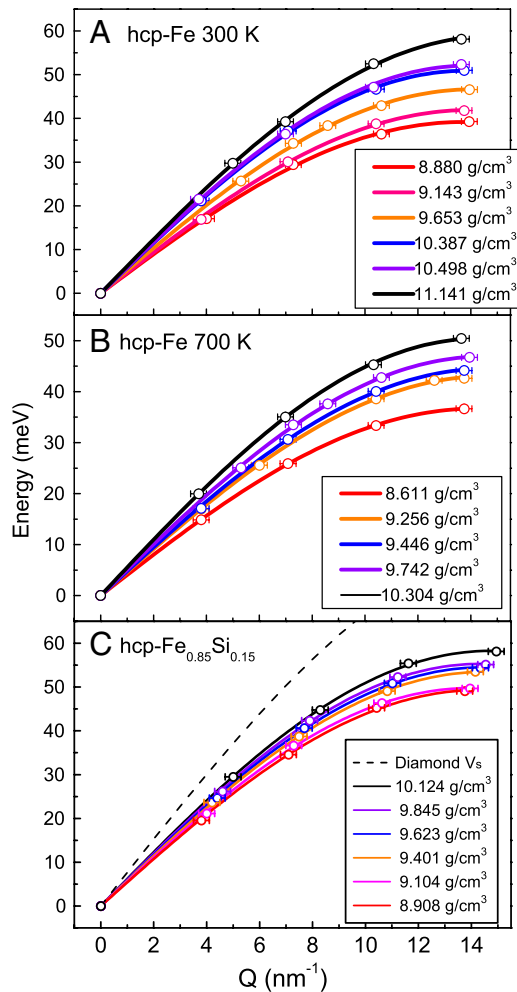
Fig. S1. Phonon dispersion curves of hcp-Fe (*A*, *B*) and hcp-$Fe_{0.85}Si_{0.15}$ at high *P-T*. (*A*) hcp-Fe at 300 K. (*B*) hcp-Fe at 700 K; (*C*) hcp-$Fe_{0.85}Si_{0.15}$ at 300 K. The measured momentum-energy (Q-E) relations were fitted using a sine function (9). The momentum and energy transfers at the origin of the Brillouin zone are intrinsically set at zero for the data analyses. Error bars of the Q are typically around 0.7 nm^{-1}, whereas uncertainties on the energy transfers are mostly less than 1%. Errors smaller than the symbols are not shown for clarity.
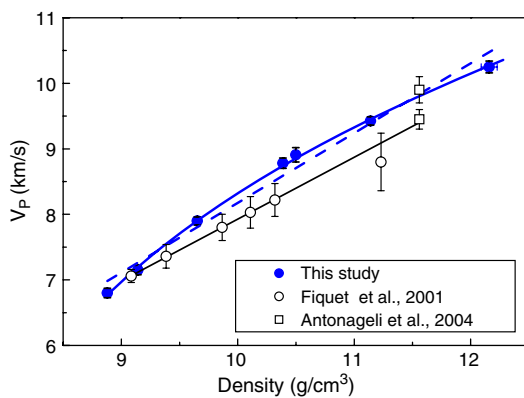
Fig. S2. Compressional-wave velocity (V_P) of hcp-Fe compared with two previous high-energy resolution inelastic X-ray scattering (HERIX) studies. Blue circles: this study at 300 K; open circles: Fiquet et al. (9); open squares: Antonangeli et al. (10). Blue solid and dashed lines represent the power-law fit and linear fit to our data, respectively, whereas black solid line represents linear fit to the data from Fiquet et al.(9).

Table S1. Measured $V_P - \rho$ of hcp-Fe

300 K				700 K			
ρ (g/cm^3)	V_P (km/s)	P (GPa)*	P medium	ρ (g/cm^3)	V_P (km/s)	P (GPa)†	P medium
8.880 (±0.010)	6.80 (±0.07)	14.4 (±0.8)	NaCl	8.611 (±0.003)	6.14 (±0.01)	11.1 (±1.0)	NaCl
9.143 (±0.003)	7.15 (±0.07)	21.7 (±0.9)	NaCl	9.256 (±0.004)	9.68 (±0.04)	26.9 (±1.5)	NaCl
9.653 (±0.005)	7.90 (±0.06)	38.0 (±1.8)	NaCl	9.446 (±0.001)	7.24 (±0.06)	32.4 (±1.7)	NaCl
10.387 (±0.005)	8.78 (±0.08)	67.2 (±2.8)	Ne	9.742 (±0.004)	7.79 (±0.07)	42.1 (±2.1)	NaCl
10.498 (±0.011)	8.91 (±0.11)	72.2 (±4.1)	Ne	10.304 (±0.004)	8.29 (±0.03)	67.1 (±2.6)	Ne
11.141 (±0.008)	9.42 (±0.06)	104.6 (±4.5)	NaCl				

*EoS of hcp-Fe from Dewaele et al. (1) was used for calculating pressures at high pressures and 300 K.
†EoS of hcp-Fe from Uchida et al. (2) was used for calculating pressures at high P-T.

1 Dewaele A et al. (2006) Quasihydrostatic equation of state of iron above 2 Mbar. *Phys Rev Lett* 97:215504.
2 Uchida T, Wang Y, Rivers ML, Sutton SR (2001) Stability field and thermal equation of state of ε-iron determined by synchrotron X-ray diffraction in a multianvil apparatus. *J Geophys Res* 106:21799–21810.

Table S2. hcp-Fe$_{0.85}$Si$_{0.15}$

300 K			
ρ (g/cm^3)	V_P (km/s)	P* (GPa)	P medium
8.908 (±0.008)	8.21 (±0.07)	39.1 (±1.5)	Ne
9.104 (±0.008)	8.49 (±0.07)	46.9 (±1.8)	Ne
9.401 (±0.004)	8.78 (±0.03)	59.9 (±2.1)	Ne
9.623 (±0.005)	8.99 (±0.06)	70.7 (±3.4)	Ne
9.845 (±0.005)	9.23 (±0.08)	82.3 (±3.7)	Ne
10.124 (±0.007)	9.42 (±0.06)	98.2 (±4.3)	Ne

*EoS from Lin et al. (1) was used for calculating pressures.

1 Lin JF, Campbell AJ, Heinz DL (2003) Static compression of iron-silicon alloys: Implications for silicon in the Earth's core. *J Geophys Res* 108:2045.